Hacettepe Üniversitesi Yerbilimleri Uygulama ve Araştırma Merkezi Bülteni (Bulletin of the Earth Sciences Application and Research Centre of Hacettepe University



Comparison between grid tomography and horizon-based tomography in prestack depth migration (PSDM)

Yığma Öncesi Derinlik Migrasyonunda (PSDM) grid tomografi ve tabaka bazlı tomografi karşılaştırmaları

SELİN CEREN 1*0, YELİZ İŞCAN ALP 20, HAKAN ALP 30

- 1,3 İstanbul Üniversitesi-Cerrahpaşa, Mühendislik Fakültesi, Jeofizik Mühendisliği Bölümü İstanbul, Türkiye
- ² İstanbul Üniversitesi-Cerrahpaşa, Teknik Bilimler Meslek Yüksekokulu, Sualtı Teknolojisi Programı, İstanbul, Türkiye

Received (geliş): 7 Nisan (April) 2025 Accepted (kabul): 1 Temmuz (July) 2025

ÖZ

In this study, the pre-stack depth migration method was applied to obtain a depth section that provides the closest approach to the subsurface. PSDM, is now used as a processing method in many seismic explorations because of the increase of the hardware and related software capabilities. In geologically and tectonically complex study areas, depth migration is essential to obtain accurate subsurface depth images. Therefore, after deriving the initial interval velocity depth section, both post-stack and prestack depth migration techniques were applied to improve subsurface imaging accuracy. Non-flatness in common depth point (CDP) gathers from PSDM indicated the need to update the interval velocity model in depth. Grid tomography and horizon-based tomography were used to refine the interval velocity depth section. PSDM was then reapplied using the updated velocity model. These steps were iteratively repeated until the CDP gathers were flattened. Grid tomography was applied twice to update the interval velocity depth section. However, analysis of the depth section from the second PSDM iteration (using grid tomography-derived velocities) showed that deeper reflections remained poorly resolved. Consequently, five additional PSDM iterations were performed with horizon-based tomography-updated velocities, resulting in significantly improved imaging of both shallow layers and the basement. Finally, depth sections from post-stack depth migration, initial PSDM, and subsequent PSDM iterations were compared to highlight the critical role of PSDM in achieving a geologically realistic model.

Anahtar Kelimeler: Grid Tomography, Horizon-based Tomography, Prestack Depth Migration, Seismic Data Processing

ABSTRACT

Bu çalışmada yeraltına dair en yakın yaklaşımı sağlayan derinlik kesiti elde edebilmek için yığma öncesi derinlik migrasyonu (PSDM) yöntemi uygulanmıştır. PSDM, donanım ve ilgili yazılım kabiliyetlerinin artması nedeniyle artık birçok sismik araştırmada bir veri işlem yöntemi olarak kullanılmaktadır. Jeolojik ve tektonik olarak karmaşık araştırma alanlarında, doğru yeraltı derinlik kesitleri elde etmek için derinlik migrasyonu

esastır. Bu nedenle, ilk olarak ara hız derinlik kesiti üretildikten sonra, hem yığma sonrası hem de yığma öncesi derinlik migrasyonu yöntemleri, yeraltı görüntüleme doğruluğunu artırmak için uygulanmıştır. PSDM sonucu elde edilen CDP gruplarında yatay olmama durumu, ara hız modelinin güncellenmesi ihtiyacını göstermiştir. Ara hız derinlik kesitini güncelleyebilmek için grid tomografi ve tabaka-tabanlı tomografi yöntemleri kullanılmıştır. Sonraki adımda, PSDM yöntemi, güncellenmiş hız modeli kullanılarak CDP grupları tamamen yatay hale gelene kadar yinelemeli olarak tekrarlanmıştır. Ara hız derinlik kesitini güncelleyebilmek için grid tomografi yöntemi iki kez uygulanmıştır. İkinci PSDM yinelemesinden elde edilen derinlik kesitinin analizi, daha derin yansımaların çözünürlüğünün hala düşük olduğunu göstermiştir. Ancak, tabaka-tabanlı tomografi ile güncellenen hızlar kullanılarak PSDM yöntemi 5. yinelemeye kadar devam ettirildiğinde, hem sığ katmanların hem de temel kayanın görüntülenmesinde önemli ölçüde iyileşme sağlanmıştır. Son olarak, yığma sonrası derinlik migrasyonu sonucu elde edilen derinlik kesiti, ilksel PSDM sonucu elde edilen derinlik kesiti ve PSDM güncellemelerinde elde edilen derinlik kesitleri arasındaki karşılaştırmalar yapılarak, PSDM yönteminin doğru ara hız modeli ve derinlik kesiti elde etmede önemi vurgulanmıştır.

Keywords: Grid Tomografi, Tabaka-tabanlı Tomografi, Yığma Öncesi Derinlik Migrasyonu, Sismik Veri İşlem

https://doi.org/10.17824/yerbilimleri.1664420

*Sorumlu Yazar/ Corresponding Author:yeliziscanalp@iuc.edu.tr

INTRODUCTION

Migration is used to replace reflections to their correct vertical and horizontal positions (Bruno, 2023; Biondi, 2006; Sheriff and Geldart, 1983). The unmigrated stack section does not reflect the real subsurface. The velocities used in Normal Move-out (NMO) correction are offsetdependent, and only horizontal layers can be imaged accurately because of the hyperbolic assumption. In the presence of dipping layers and complex structures, events can be mispositioned. Therefore, migration is necessary to locate reflections in their correct positions. The selection of migration type is dependent on the geology of the area. When the subsurface is not complex, it is better to apply time migration (Yılmaz, 2001). However, time migration uses RMS velocity models that do not allow ray bending at layer boundaries; this situation can cause lateral mispositioning of the reflection events. For this reason, in the presence of lateral velocity variations and complex structures (salt domes, faults, overthrust), depth migration is required. Post-stack migration is convenient in the presence of a horizontal layer, because this

method assumes that the stack section is similar to a zero-offset section. However, when there are conflicting dips, the stack section is not similar to the zero-offset section. In the post-stack migration, reflection events with non-hyperbolic moveout can be distorted (Bruno, 2023; Yılmaz, 2001). In this case, prestack migration is needed. Prestack depth migration yields a better subsurface image in the presence of conflicting dips, lateral velocity variations, and complex structures. In this study, prestack depth migration was applied iteratively to obtain a better image of the subsurface. This study aims to emphasize the importance of the true interval velocity depth model, to obtain a depth section close to real geology, to view stratigraphic elements in their correct vertical and horizontal location, and to increase the resolution of the depth section to interpret layers. In the application of prestack depth migration, 2D Kirchhoff migration was used. This method can give better results because it handles irregularities in the data when compared to other methods (Rastogi, 2015;

Schneider, 1978). This method is based on the summation of scaled amplitudes along computed diffraction curves that are based on an integral solution to the scalar wave equation. The velocity model for prestack depth migration is so important to obtain high resolution subsurface image. The interval velocity depth model is used in PSDM. The interval velocity depth model contains the full complexity of the area because it uses actual ray paths from every source and every receiver to each subsurface point and allows ray bending at layer boundaries.

MATERIAL AND METHOD

Routine Data Processing Steps

In this study, multichannel seismic data collected by TPAO were used and processed via Echos-Paradigm software. The seismic data includes 120 channels. The shot interval and group interval are 26,67 m, the sampling rate is 2 ms, the record length is 7000 ms and the near offset is 160 m. The routine data processing steps applied to the data are data loading, editing, muting, bandpass filtering, predictive deconvolution, f-k filter, CDP sorting, and velocity analysis, as shown by the flowchart in Figure 1. The bandpass filter frequencies were optimally selected as 2-5-130-135 Hz through comprehensive analysis of shot gather amplitude spectra, ensuring preservation of all relevant signal components (Figure 2a). As shown in Figure 2a, the high-frequency noise at 160 Hz, attributed to operational noise, was filtered out after the application of the bandpass filter. In the predictive deconvolution process, the operator length and prediction lag are important (Dondurur, 2018). For this reason, by analyzing the autocorrelation function, the operator length and prediction lag were selected as 100 ms and 24 ms, respectively (Figure 2b). In the f-k filter, noises like refraction waves, direct waves, and back-scattered waves are close to the wavenumber axis. Therefore, these regions should be filtered. By analyzing f-k spectrum, the low dip and high dip rates were selected as -12 and 12 (ms/trace) respectively (Figure 2c). These rates were not selected too high, because when

high parameters were selected, it caused signal loss. However, the aliased energy remained, due to dip rate selection.

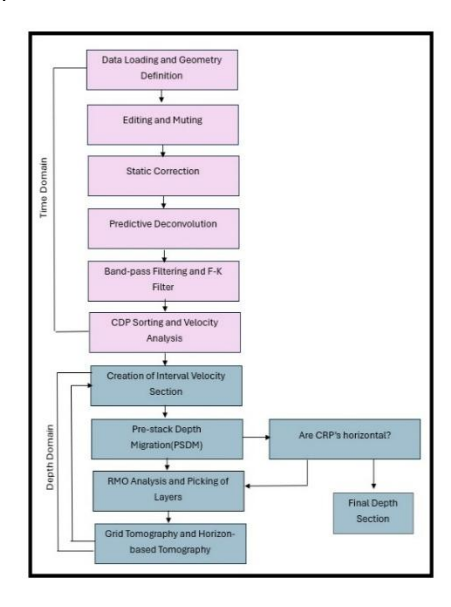


Figure 1. Flowchart of seismic data processing applied in this study.

Şekil 1. Çalışmada uygulanan sismik veri işlem akış şeması.

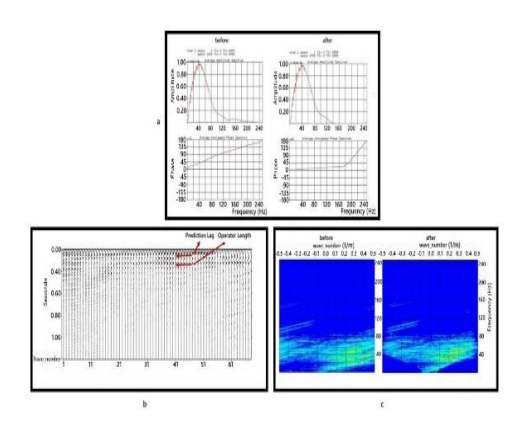


Figure 2. a) Amplitude spectrum images before and after applying the band-pass filter; b) selection of operator length and prediction lag based on autocorrelation function analysis; c) images before and after applying the f-k filter.

Şekil 2. a) Bant geçişli süzgeçleme uygulanmadan önce ve uygulandıktan sonra genlik spektrum görüntüleri; b) Otokorelasyon fonksiyonu analizine dayalı operatör uzunluğu ve kestitim uzaklığı seçimi; c) f-k filtresi uygulanmadan önce ve sonra elde elde edilen spektrumların görünümü.

Application of Prestack-Depth Migration (PSDM) Method

Kirchhoff migration is an integral solution to scalar wave equation. Audebert (1997) evaluated migration methods for use as practical implementation and defined Kirchhoff migration as the best method. This method can be defined by Huygen's principle. According to this principle, seismic reflectors are composed of closely spaced depth points. Huygen's secondary source corresponds to semicircles in the depth domain and hyperboles in the time domain (Yılmaz. 2001). The integral solution to scalar wave equation is used in the practical implementation of the Kirchhoff migration based on diffraction summation (Richa Rastogi, 2017; Yılmaz, 2001). The summation approach can handle more irregular contents of data compared with other methods (Schneider, 1978). The geometry of the diffraction hyperbola depends on the rays traveling from the diffraction point to the receiver points at the surface.

$$\left| \frac{d^2}{dx^2} + \frac{d^2}{dz^2} - \frac{1}{V(x,z)^2} \frac{d^2}{dt^2} \right| P(x,z;t) = 0 \tag{1}$$

$$P_{out}(x_0, z) = \frac{\Delta x}{2\pi} \sum_{x} \left[\frac{\cos \theta}{\sqrt{Vx}} p(t) * P_{in}(x, z = 0, t) \right]$$
 (2)

Equation 1 is the scaler wave equation, P(x, z=0)t) is the input wavefield and V (x, z) is the velocity of the medium. Equation 2 is the discrete form of the integral solution to the scalar wave equation (Yılmaz, 2001). In equation 2, traveltimes are calculated from every receiver and source for each subsurface points. According to this equation $r = \sqrt{(x - x_0)^2 + z^2}$ is the distance between the observation and imaging point. The rho filter p(t) is the time derivative of the input wavefield. In the application of the 2D migration half derivative of the measured wavefield is used. $Cos(\theta)$ is an obliquity factor that defines the angle dependence of the amplitudes and $1/\sqrt{Vr}$ is proportional to spherical factor. Pout (x, z=VT/2, t=0) is output wavefield at subsurface location (x₀, z). In this study, time domain RMS velocity section was converted to interval velocity depth section via Dix conversion. RMS velocity section and interval velocity depth section is shown in the Figure 3 and Figure 4, respectively.

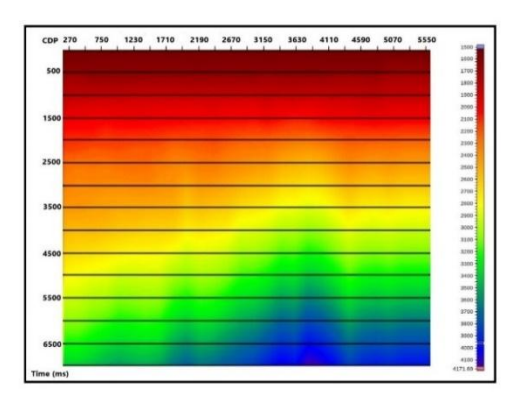


Figure 3 Image of the RMS velocity time section.

Şekil 3. Zaman ortamı RMS hız kesiti.

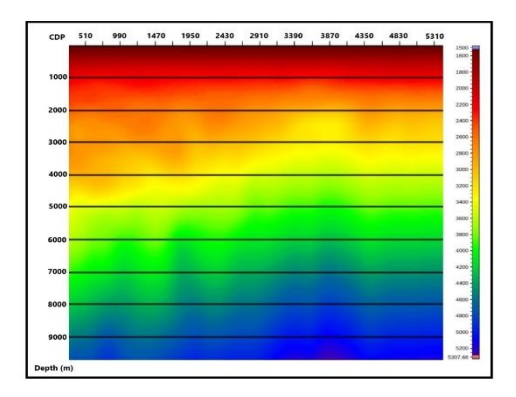


Figure 4. Image of the initial interval velocity depth section.

Şekil 4. Ara hız kesiti görünümü.

Then 2D Kirchhoff prestack depth migration was applied to the data. Aperture value selection is so important in the implementation of the Kirchhoff migration (Schleicher et al., 1997). While high aperture values correspond to more computer run time, low values correspond to a poor image (Rastogi et al., 2000). Therefore, in this study, the PSDM method was applied with aperture values that vary with depth. It was realized that the resolution of the depth section increased when the aperture value was high. However, it is necessary to consider that when the aperture value is too high, it can cause amplitude loss in the shallow layers. Figure 5 shows a comparison of the depth sections with aperture lengths of 4000 m and 10000 m for depths of up to 10500m. According to this comparison, an appropriate aperture length of 500 m for depth of up to 300 m and an aperture length of 10000 m for depths of up to 10500 m was selected. In the Figure 6, depth section obtained from initial PSDM using parameters described in Table 1 is shown.

Table 1. The selection of the aperture lengths for depths of up to 300 m and 105000 m.

Tablo 1. 300 m ve 10500 m derinliğe kadar yarı açıklık genişliği değeri seçimi.

Depth(m)	Aperture Length(m)
300	500
10500	10000

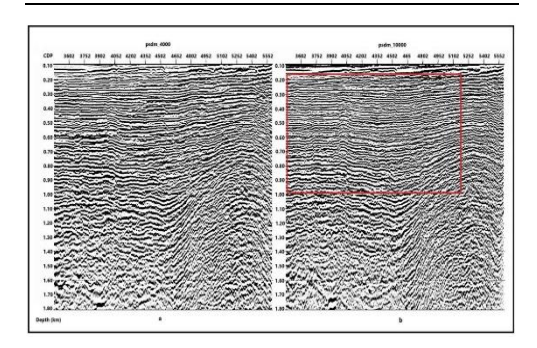


Figure 5. Application of Pre-Stack Depth Migration (PSDM) with aperture lengths of a) 4000 m and b) 10000 m for depths of up to 10500 m.

Şekil 5. 10500 m'ye kadar derinlikler için a) 4000 m ve b) 10000 m yarı açıklık genişliği değerleri ile yığma öncesi derinlik migrasyonu uygulaması.

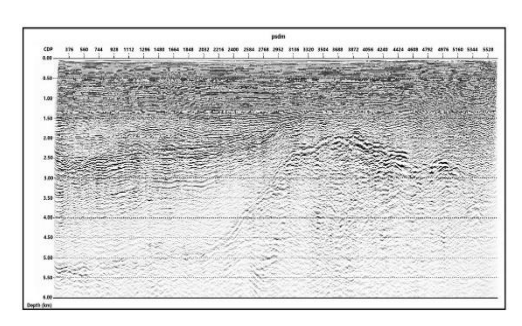


Figure 6. Initial depth section obtained from first iteration of PSDM.

Şekil 6. PSDM'nin ilk uygulamasından sonra elde edilen başlangıç derinlik kesiti.

Grid Tomography and Horizon-Based Tomography

If the initial interval velocity depth section is not accurate, there can be residual moveouts in the CDP gathers (Tian-wen Lo et.al, 1994) (Figure 7). The velocity model updating in PSDM method is based on reflection travel time tomography that use Residual Moveout Analysis (RMO) (Stork, 1992; Wang and Pratt, 1997; Woodward, 2008). Velocity model updating is based on RMO that requires careful picking in the gathers (Woodward et al., 2008). This method is based on the principle of obtaining the minimum difference between the observed travel times and the modeled travel times via the inverse solution of the process (Bruno, 2023; Yılmaz, 2001; Sherwood et al., 1986; Kosloff et al., 1996). In this study, grid tomography and horizon-based tomography were used to update the interval velocity depth model.

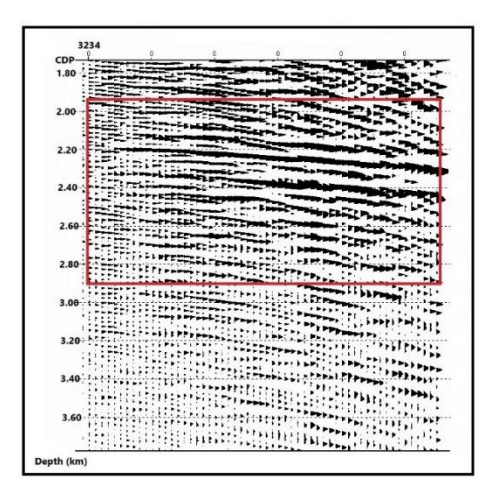


Figure 7. Initial CDP gathers obtained from first iteration of PSDM.

Şekil 7. İlk PSDM yinelemesinden elde edilen CDP grupları.

Both methods employ simultaneous equation systems to compute updated model parameters. The methods differ in their spatial distribution of input data and the pattern of parameter updates. Grid tomography that requires an interval velocity depth section and interpreted horizons updates velocities at equally spaced grid points. As in

horizon-based tomography, depth reflectors are used as a ray tracing grid source in grid tomography. On the other hand, horizon-based tomography requires a velocity-depth model to update both the velocity and depth of the reflector for each horizon. Horizon-based tomography offers several advantages over grid tomography, particularly in generating more geologically realistic velocity-depth models. This approach achieves superior results by updating velocity parameters independently for each interpreted horizon. Additionally, the drawback of the grid tomography is that even low relative residual RMS velocity selection rates can create artificial folding in the depth section. However, in the presence of complex structures, it can be difficult to define formation bottoms for use as ray-tracing sources. Therefore, in this study, grid tomography was applied before horizon-based tomography. The error in time at the CMP location can correspond to errors in the velocity for grid tomography and errors in both depth and velocity for horizon-based tomography. In the equation (3); t'(n) is the modeled traveltime, (z - zk-1) is the depth of the layer, S_k is the slowness (1/V_k) and θ is the angle made with the vertical axis (Yılmaz, 2001). In the equation (4), t_{initial} is the initial traveltimes, t'(n) is the modeled traveltimes and t(n)observed is the observed traveltimes. In the equation (5) e(n) is the difference between observed traveltimes and modeled traveltimes.

$$t'(n)=(z_k-z_{k-1}) S_k \sec \theta$$
 (3)

$$t'(n)_{modeled} = t'(n)_{initial} + \frac{dt'_n}{dp} \Delta p$$
 (4)

$$e(n)=t(n)_{observed}-t(n)_{modeled}$$
 (5)

$$e(n)=\Delta t-\Delta t'$$
 (6)

$$\Delta t = \frac{dt r_n}{dp} \Delta p \tag{7}$$

$$\Delta t' = L\Delta p$$
 (8)

In the equation (8) $\Delta t'$ is the column vector, L is the sparse matrix($\frac{dt r_n}{dp}$) and Δp is the column vector.

According to equation (6) using least squares, the solution is achieved.

$$\Delta p = (L^{T}L)^{-1}L^{T}\Delta t \tag{9}$$

According to equation (9), Δt is the residual moveouts measured from gathers, L is the sparse matrix that represents first derivative of the parameters. Using equation (9) Δp is calculated and then parameter is updated (p+ Δp). First, in the velocity updating process, horizons interpreted for use as a ray tracing source (Cerveny and Soares, 1992). The image of the picking of the interpreted horizons is shown in Figure 8.

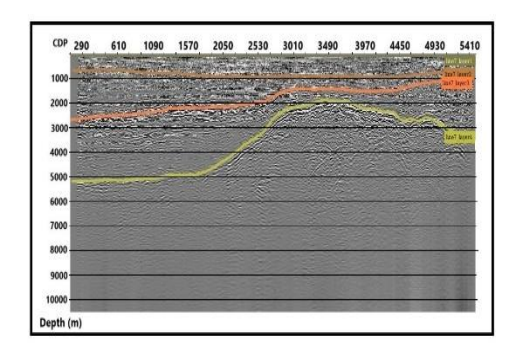


Figure 8. The image of the interpreted horizons.

Şekil 8. Yorumlanan tabakaların görünümü.

In grid tomography, to create a travel time error source relative residual RMS velocity picking was applied to the velocity panel of the spectrum. Figure 9 a-b shows the velocity panel and the CDP groups, respectively. The vertical axis of the velocity panel represents the depth of events, and the horizontal axis represents the relative residual RMS velocity. Residual moveouts in CDPs

change according to velocity selection. When the true velocities are selected, CDPs become flat. After the picking of semblances in the velocity panel, the RMS residual section was created (Figure 10).

The RMS residual section, interpreted horizons, and the initial interval velocity depth section were used as inputs for grid tomography. In grid tomography, smaller grid spacing yields higher accuracy and resolution in the results. Therefore, a grid step (horizontal shooting grid) of 13 m and a ray step (depth step) of 10 m were adopted. After the second iteration of the grid tomography, an updated interval velocity depth section was created (Figure 11).

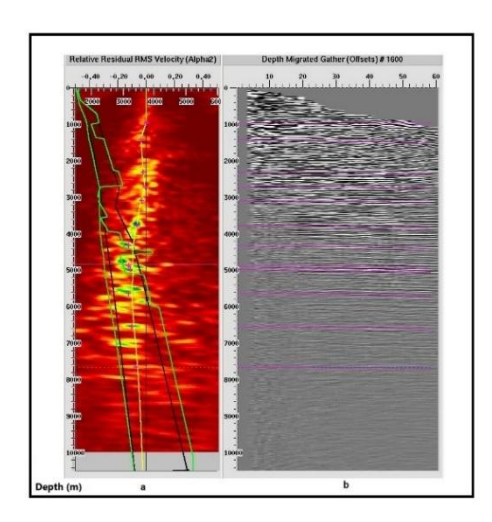


Figure 9. The image of the Residual RMS velocity selection. a) Residual moveout semblance spectra computed from CDP gathers, b) CDP gathers derived from PSDM. Selected residual RMS velocities, reference velocities previously assigned to interpreted horizons and interval velocities of events at depths are shown with yellow line, black line and green line respectively.

Şekil 9. Kalıntı RMS hız seçimi görünümü. a) CDP gruplarından hesaplanan kalıntı kayma spektrumu, b) PSDM sonucu elde edilen CDP grupları. Seçilen kalıntı RMS hızları, daha önce yorumlanmış tabakalara atanan referans hızları ve derinliklerdeki ara hızları sırasıyla sarı çizgi, siyah çizgi ve yeşil çizgi ile gösterilmiştir.

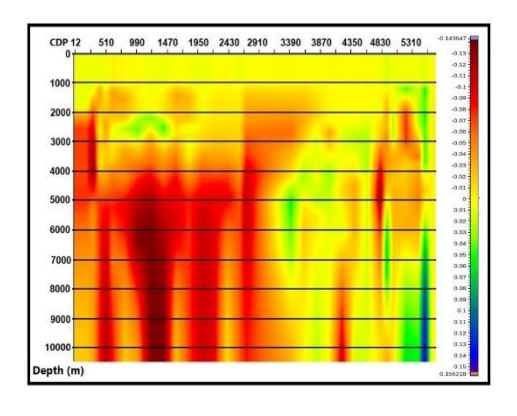


Figure 10. Relative Residual RMS velocity section obtained from the RMO analysis.

Şekil 10. RMO analizinden elde edilen bağıl kalıntı RMS hız kesiti.

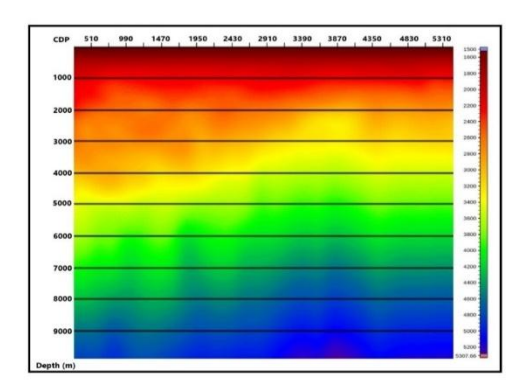


Figure 11: Updated interval velocity depth section after second iteration of grid tomography.

Şekil 11: Grid tomografi ile 2. Güncelleme sonucu elde edilen ara hız kesiti.

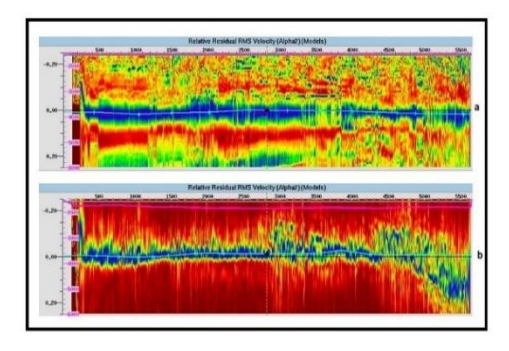


Figure 12. Residual moveout analysis for a) horizon and b) horizon2.

Şekil 12. Tabaka tabanlı tomografide tabaka 1 ve 2 için kalıntı kayma analizi.

Horizon-based tomography was then applied to derive a geologically realistic interval velocity depth section and reduce residual moveouts in CDPs. The inputs for horizon-based tomography are the interval velocity depth section obtained from the second iteration of grid tomography, interpreted horizons, and RMO pickings for each horizon. The vertical axis of Figure 12 represents the depth error of the horizon that corresponds to the relative residual RMS velocity. After relative residual RMS velocities were selected, an updated interval velocity depth section was created. Finally, Figure 13 shows the interval velocity depth section obtained from the fifth iteration of horizon-based tomography.

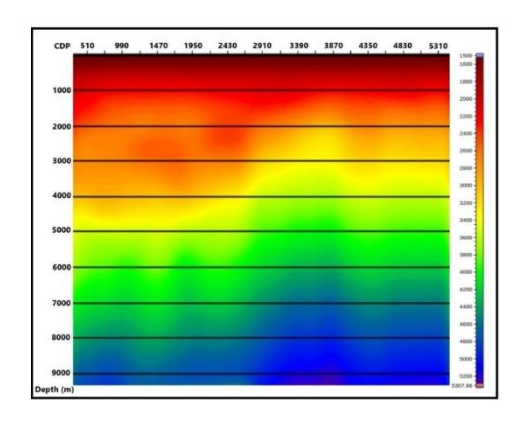


Figure 13. Updated interval velocity section obtained from fifth iteration of horizon-based tomography.

Şekil 13. Tabaka tabanlı tomografi ile 5. güncelleme sonucu elde edilen ara hız kesiti.

DISCUSSION

As a first step in this study, depth sections obtained from poststack and prestack depth migration were compared. Then, using PSDM, the initial depth section and updated depth sections were compared to each other. The iterative application of PSDM was discontinued when either excessive artificial folding of layers occurred or no further improvements were observed. This study highlights the importance of prestack depth migration (PSDM) for determining an accurate velocity model that yields optimal results in complex geological areas. A geologically realistic velocity model produces superior imaging results.

Figure 14 presents all CDP gathers from both initial and subsequent iterations, demonstrating non-flat events in the initial gathers and flattened events after velocity model updates. The CDPs became flat after further iterations. Figure 15 shows a comparison of depth sections from post-stack depth migration and PSDM. According to Figure 15, the horizons can be better distinguished, and faults can be tracked better with the application of PSDM up to 1 km depth.

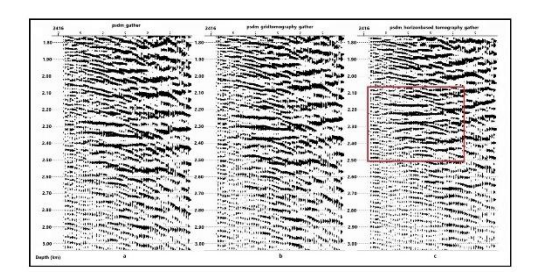


Figure 14. Image of CDP gathers obtained from a) initial PSDM b) the second iteration of PSDM using interval velocities derived from grid tomography and c) fifth iteration of PSDM using interval velocities derived from horizon-based tomography.

Şekil 14. a) Başlangıç ara hız kesiti ile uygulanan PSDM, b) grid tomografi ile güncellenen ara hızlar kullanılarak uygulanan 2. yineleme PSDM ve c) tabakatabanlı tomografi ile güncellenmiş ara hızlar kullanılarak uygulanan 5. yineleme PSDM sonucu elde edilen CDP grupları görünümü.

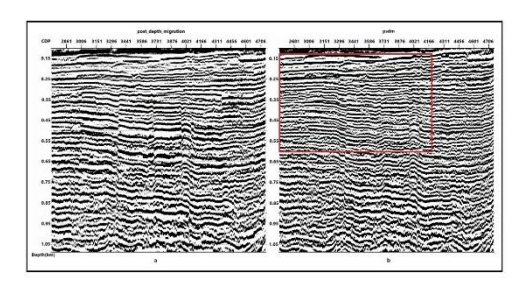


Figure 15. Image of a) depth section obtained from post stack depth migration and b) initial depth section obtained from PSDM.

Şekil 15. a) Yığma sonrası derinlik migrasyonu sonucu elde edilen derinlik kesiti ve b) PSDM sonucu elde edilen ilksel derinlik kesitinin görünümü.

The grid-tomography method was subsequently performed to update the interval velocity depth section. Performing more than two iterations of PSDM with updated interval velocities obtained through grid tomography led to excessive artificial folding in the shallow layers. Because of this, we decided to stop at the second iteration (Figure 16). In Figure 17, the initial depth section and

depth section from the second iteration of PSDM using grid tomography in interval velocity refinement are compared. Corresponding improvements in reflection amplitudes (indicated by red arrows) are evident at the basement interface in the updated depth section (Figure 17b). Furthermore, enhanced layer resolution is observed between 1.50-2.50 km depth (Figure 17d). To optimize basement delineation and shallow-layer imaging, we implemented horizonbased tomography for subsequent velocity model updates. The first input interval velocity model for horizon-based tomography is the second iteration of the interval velocity depth section updated by grid tomography. PSDM was performed six times using updated interval velocities derived from horizon-based tomography, and in the fifth iteration was stopped because there were no changes in layers in the depth section from the sixth iteration (Figure 18).

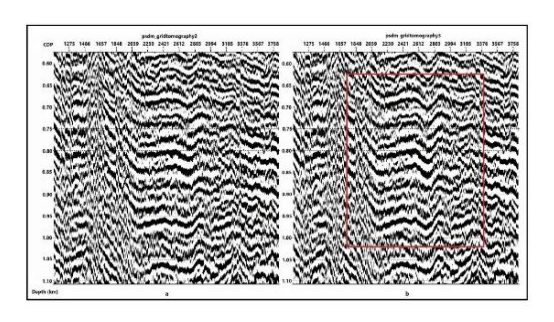
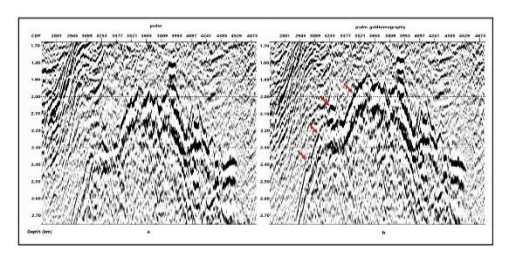


Figure 16. Comparison of images of depth sections obtained from a) second and b) third iteration of the PSDM using interval velocities derived from grid tomography.

Şekil 16. Grid tomografi ile güncellenmiş ara hızlar kullanılarak a) 2. yineleme PSDM sonucu ve b) 3. yineleme PSDM sonucu elde edilen derinlik kesitlerinin karşılaştırılması.

In Figure 19, the depth sections from the second iteration of PSDM and the fifth iteration of PSDM using grid tomography and horizon-based tomography, respectively, in interval velocity refinement, are compared. In this figure, it is seen that folding in a basement is imaged and distinguished in the depth section from the fifth iteration of PSDM. Additionally, when we analyze the comparison of colored views of depth

sections, layers are better recognized at depths between 3.75-5 km in Figure 20b.



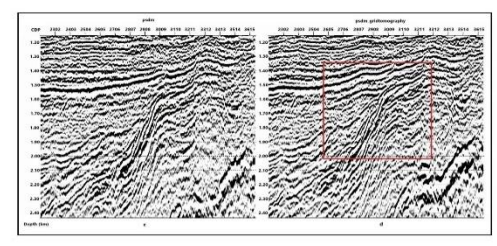


Figure 17. Comparison of images of basement in the depth sections obtained from a) initial PSDM and b) second iteration of PSDM using interval velocities derived from grid tomography. Comparison of images of shallow layers in the depth sections obtained from c) initial PSDM and d)second iteration of PSDM using interval velocities derived from grid tomography.

Şekil 17. a) İlksel PSDM sonucu ve b) grid tomografi ile güncellenmiş ara hız modeli kullanılarak 2. yineleme PSDM sonucu elde edilen derinlik kesitlerinde temel kaya görünümünün karşılaştırılması. c) İlksel PSDM sonucu ve d) grid tomografi ile güncellenmiş ara hız modeli kullanılarak 2. yineleme PSDM sonucu elde edilen derinlik kesitlerinde sığ tabakaların görünümünün karşılaştırılması.

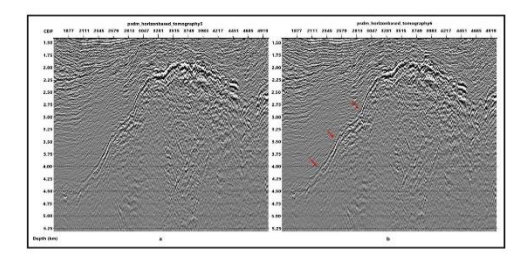


Figure 18. Image of the depth sections obtained from a) fifth and b) sixth iteration of PSDM using interval velocities derived from horizon-based tomography.

Şekil 18. Tabaka-tabanlı tomografi ile güncellenmiş ara hızlar ile uygulanan a) 5. yineleme PSDM ve b) 6. yineleme PSDM sonucu elde edilen derinlik kesitlerinin karşılaştırılması.

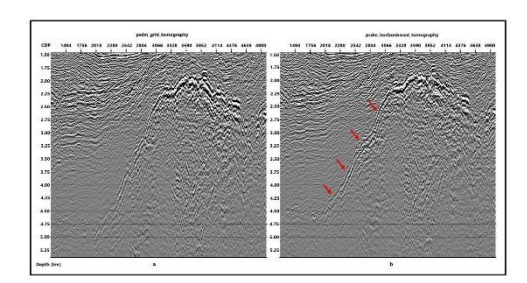


Figure 19. Comparison of depth sections from the a) second iteration of PSDM and b) fifth iteration of PSDM, utilizing interval velocities derived from grid tomography and horizon-based tomography, respectively.

Şekil 19. a) Grid tomografi ile güncellenmiş ara hızlar ile uygulanan 2. yineleme PSDM sonucu ve b) tabakatabanlı tomografi ile güncellenmiş ara hızlar ile uygulanan 5. yineleme PSDM sonucu elde edilen derinlik kesitlerinin karsılastırılması.

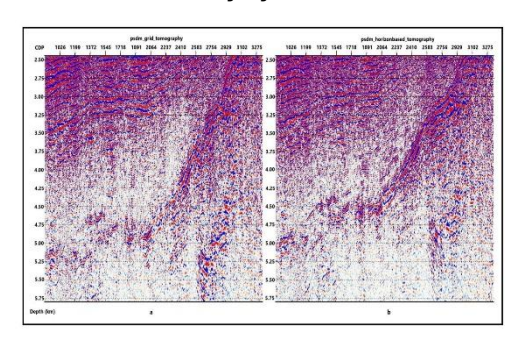


Figure 20. Comparison of colored depth sections from the a) second iteration of PSDM and b) fifth iteration of PSDM, utilizing interval velocities derived from grid tomography and horizon-based tomography, respectively.

Şekil 20. a) Grid tomografi ile güncellenmiş ara hızlar ile uygulanan 2. yineleme PSDM sonucu ve b) tabakatabanlı tomografi ile güncellenmiş ara hızlar ile uygulanan 5. yineleme PSDM sonucu elde edilen derinlik kesitlerinin renkli görünümlerinin karşılaştırılması.

Figure 21b demonstrates proper layer positioning with complete elimination of grid-tomography-induced folding artifacts, particularly in the upper 1 km section. In Figure 22, the initial depth section and updated depth sections using grid tomography and horizon-based tomography in interval velocity refinement are compared to each

other. According to Figure 22b-c, positioning changes are observed, especially at depths of 0.60-1.00 km. There is folding in layers in Figure 22b, and the dip of the layers increased after the fifth iteration of PSDM shown in Figure 22c. Furthermore, Figure 22 demonstrates that the 1.5 km horizon in the initial PSDM section appears deeper than its position in the updated depth sections, as indicated by the red arrows.

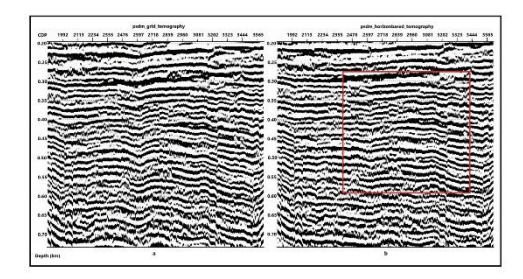


Figure 21. Comparison of shallow layers in the depth sections from the a) second iteration of PSDM and b) fifth iteration of PSDM, utilizing interval velocities derived from grid tomography and horizon-based tomography, respectively.

Şekil 21. a) Grid tomografi ile güncellenmiş ara hızlar ile uygulanan 2. yineleme PSDM sonucu ve b) tabakatabanlı tomografi ile güncellenmiş ara hızlar ile uygulanan 5. yineleme PSDM sonucu elde edilen derinlik kesitlerinde sığ tabakaların karşılaştırılması.

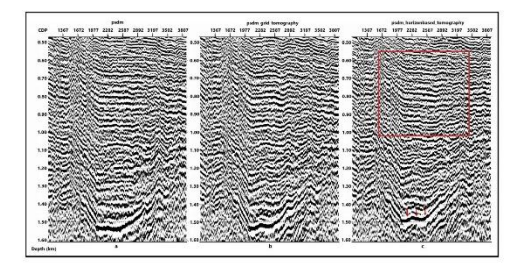


Figure 22. Comparison of shallow-layers in the depth sections from a) the initial PSDM, b) the second iteration of PSDM, and c) the fifth iteration of PSDM, utilizing interval velocities derived from grid tomography and horizon-based tomography, respectively.

Şekil 22. a) İlksel PSDM sonucu, b) grid tomografi ile güncellenmiş ara hızlar ile uygulanan 2. yineleme PSDM sonucu ve c) tabaka-tabanlı tomografi ile güncellenmiş ara hızlar ile uygulanan 5. yineleme PSDM sonucu elde edilen derinlik kesitlerinde sığ tabakaların karşılaştırılması.

The top of the basement is observed at depths of 2.00 km in Figure 23a, 1.90 km in Figure 23b, and 1.80 km in Figure 23c. As a result, to obtain a true, realistic depth image of the subsurface, PSDM is highly important. Because PSDM is dependent on the velocity model, it is important to obtain a true velocity-depth model. For this reason, updating the interval velocity section contributes to a better image of the subsurface. In conclusion, horizon-based tomography proved most effective for updating the interval velocity model. Using these updated velocities in the PSDM process resulted in a more accurate and geologically realistic depth section.

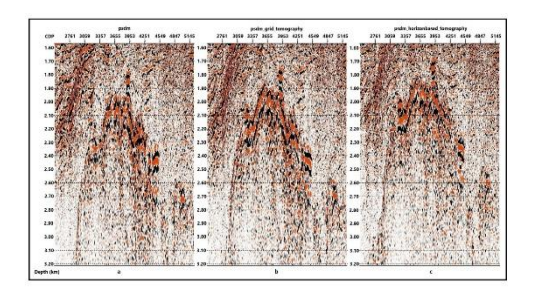


Figure 23. Comparison of basement in the depth sections from a) the initial PSDM, b) the second iteration of PSDM, and c) the fifth iteration of PSDM, utilizing interval velocities derived from grid tomography and horizon-based tomography, respectively.

Şekil 23. a) İlksel PSDM sonucu, b) grid tomografi ile güncellenmiş ara hızlar ile uygulanan 2. yineleme PSDM sonucu ve c) tabaka-tabanlı tomografi ile güncellenmiş ara hızlar ile uygulanan 5. yineleme PSDM sonucu elde edilen derinlik kesitlerinde temel kayanın karşılaştırılması

CONCLUSION

The iterative application of the prestack depth migration (PSDM) combined with velocity model refinement via grid and horizon-based tomography demonstrates the critical role of accurate velocity modeling in resolving complex subsurface structures. In this study, the superiority of PSDM over post-stack depth migration is evident, particularly in areas with lateral velocity variations and steeply dipping reflectors. Post-stack depth migration, reliant on simplified velocity assumptions, fails to account

for ray-path bending and non-hyperbolic moveout, leading to mispositioned events and reduced resolution (Yılmaz, 2001). By contrast, PSDM using interval velocities derived from iterative tomography, enables precise imaging of geological features such as folds, faults, and basement structures. The initial velocity model, generated via Dix conversion of RMS velocities, provided a starting point but inherently lacked the resolution to capture lateral velocity gradients. Subsequent application of grid tomography enhanced shallow imaging through global velocity adjustments but proved insufficient for resolving deeper targets, particularly the basement. This aligns with known challenges of grid-based methods, which often oversmooth velocity gradients and lack geological constraints (Jones, 2010). Excessive PSDM application (>2 iterations) with grid tomography-updated interval velocities induced artificial folding artifacts in shallow layers, demonstrating the risks of overautomated velocity updates. In contrast, the fifth iteration employing horizon-based tomography for velocity refinement became crucial for resolving deeper structures. The fifth PSDM iteration significantly improved imaging quality throughout the section, enhancing both shallow-layer resolution and basement definition while addressing reflectivity ambiguities and amplitude fidelity (Figures 19-21). The CDP gathers after iterative velocity updates (Figure 14), validates the convergence of the velocity model toward geological plausibility. Residual moveout in initial CMP gathers indicated velocity model inaccuracies, while progressive flattening of gathers confirmed the reduction of travel-time errors through successive iterations. Notably, the final depth section revealed repositioned horizons (e.g., basement shifted below 1.70 km; Figure 23), emphasizing the dynamic interplay between velocity refinement and structural repositioning.

ACKNOWLEDGMENT

This manuscript is a part of Selin Ceren's Ph.D thesis. This study was supported by the Scientific and Technological Research Council of Turkey (TUBİTAK 121Y405) and Istanbul University – Cerrahpasa Scientific Research Project FOA-2024-37535. We used the Echos Paradigm

software. We thank the Educational Grant Program for providing a free license to IU-C Department of Geophysical Engineering for the use of the package processing software for educational and research purposes. We are deeply grateful to the anonymous reviewers for their insightful comments and thoughtful recommendations, which helped us enhance the rigor and clarity of this manuscript.

REFERENCES

- Audebert F, Nichols D, Rekdal T, Biondi B, Lumley DE, Urdaneta H (1997). Imaging complex geologic structure with single-arrival Kirchhoff prestack depth migration, Geophysics, 62, 1533–1543, doi:10.1190/ 1.1444256.
- Biondi B (2006). Prestack exploding-reflectors modeling for migration velocity analysis, SEG Technical Program Expanded Abstracts, 25, 3056.
- Bruno PP (2023). Seismic exploration methods for structural studies and for active fault characterization: a review, DOI: 10.3390/app13169473.
- Dondurur D (2018). Acquisition and Processing of Marine Seismic Data, ISBN: 978-0-12-811490-2 https://doi.org/10.1016/C2016-0-01591-7 Elsevier Pub. Pages 493-547
- Jones IF (2003). Velocity modeling for depth migration. Geophysical Prospecting, 51 (5), 435–442.
- Kosloff D, Sherwood J, Koren Z, Machet E, Falkovitz Y (1996). Velocity and interfaces depth determination by tomography of depth migrated gathers, Geophysics, 61, 1511-1523
- Levin FK (1971). Apparent velocity from dipping interface reflections, Geophysics, 36, 510-516.
- Rostagi R, Londhe A, Srivastava A, Sirasala K, Khonde K (2017). 3D Kirchhoff migration algorithm: A new scalable approach for

- parallelization on multicore CPU based cluster,
- Rastogi R, Srivastava A, Khonde K, Sirasala KM, Londhe A, Chavhan H (2015). An efficient parallel algorithm: Poststack and prestack Kirchhoff 3D depth migration using flexi-depth iterations.
- Rastogi R, Yerneni S, Phadke S (2000). Aperture
 Width Selection Criterion in Kirchhoff
 Migration. Association of Exploration
 Geophysicists Seminar on Exploration
 Geophysics, Goa, India.
- Schleicher J, Hubral P, Tygel M, Jaya MS (1997). Minimum apertures and fresnel zones in migration and demigration. Geophysics 62 (1), 183–194.
- Schneider W (1978). Integral formulation for migration in two and three dimensions. Geophysics 43 (1), 49–76.
- Sheriff R, Geldart L (1983). Exploration Seismology. Cambridge University Press, UK.
- Stork C (1992). Reflection tomography in the post migrated domain. Geophysics 57, 680e692. https://doi.org/10.1190/1.1443282.
- Yilmaz O (1987). Seismic Data Processing: SEG, Tulsa, p. 240-353.
- Yilmaz O (2001). Seismic Data Analysis: Processing, Inversion and Interpretation of Seismic Data, vols. 1 and 2. Society of Exploration Geophysicists, Tulsa, U.S.A.
- Tian-wen Lo and Philip Inder Weisen (1994), Fundamentals of seismic Tomography, SEG monograph series.
- Wang Y, Pratt RG (1997.) Sensitivities of seismic traveltimes and amplitudes in reflection tomography. Geophysics. J. Int. 131, 618e642. https://doi.org/10.1111/ j.1365-246X.1997.tb06603.x.
- Woodward MJ (1992). Wave-equation tomography. Geophysics 57, 15e26. https://doi.org/10.1190/1.1443179.
- Woodward MJ, Nichols D, Zdraveva O, Whitfield P, Johns T (2008). Adecadeof tomography. Geophysics 73, VE5–VE1.